

Two-dimensional model of a fault

J. M. Carlson

Department of Physics, University of California, Santa Barbara, California 93106

(Received 20 June 1991)

We present the results of simulations of a two-dimensional mechanical model of a fault, which is a generalization of the one-dimensional model studied previously [Carlson and Langer, *Phys. Rev. A* **40**, 6470 (1989)]. We incorporate both the lateral fault axis and the fault depth, and consider both cases of spatially homogeneous and depth-dependent velocity-weakening friction. Our main result is that in both cases for small- to moderate-sized events, the Gutenberg-Richter scaling exponent b is unity for a wide range of parameters, as observed in the one-dimensional model, and consistent with measurements for real earthquakes. In addition, in the depth-dependent friction model, we study the activity patterns as a function of depth. We observe that smaller events tend to be triggered near the surface, while on relatively shallow faults larger events tend to achieve their first appreciable velocities at depth, in agreement with certain trends observed in seismological studies of the hypocenter distributions of small and large earthquakes.

PACS number(s): 05.40.+j, 91.30.Px, 05.45.+b

Recently, we have investigated the dynamic behavior of a simple, homogeneous, one-dimensional model of a fault, in which the key nonlinearity is the velocity-weakening friction at the interface between tectonic plates [1–7]. One interesting result obtained in Refs. [1] and [2] was a demonstration that this spatially homogeneous model can generate a noisy spectrum of earthquakelike events: The smaller slipping events are consistent with the fundamental law governing the frequency distribution $R(\mu)$ of earthquakes of magnitude μ , namely, the Gutenberg-Richter statistical law [8]:

$$R(\mu) = Ae^{-b\mu}, \quad (1)$$

where A is a constant and $b \approx 1$, while the large events have a separate distribution. As observed in nature, for a wide range of parameters the large events occur more frequently than would be expected from an extrapolation of the statistics of smaller events on a single fault [9], although for real faults the detailed form of the distribution of large events is difficult to determine because of the sparsity of single-fault data.

In this paper we present results for generalizations of the earthquake model to higher dimensions. Previously, our studies were limited to a strictly one-dimensional version of the model. Of course, the Earth is three dimensional, and as we proceed in comparing our results to seismological data, it is particularly important to determine the effect of dimensionality on this system. In most physical systems dimensionality plays an important role in scaling properties; thus this question is of both fundamental and practical interest. Furthermore, in the Earth the material properties of the crust vary with depth [10], leading to depth-dependent features in seismicity patterns [11], which will also be discussed here.

Ultimately, it will be useful to study a fully three-dimensional version of the model. However, in large simulations an increase in dimensionality must be accom-

panied by a decrease in system length. Thus we first consider a two-dimensional version of the model, explicitly taking into account both the lateral fault axis and fault depth. Interestingly, we here report that in the two-dimensional model, with and without depth-dependent friction, the $b=1$ Gutenberg-Richter scaling [Eq. (1)] that was observed in one dimension also persists in two dimensions. In addition, as in one dimension, we observe an excess of large events above the extrapolated rate of smaller events. However, in two dimensions this excess is somewhat less pronounced.

The model we study is described in detail in Ref. [2] and is the simplest example of a class of models which was introduced over 20 years ago in the seismological literature by Burridge and Knopoff [12]. In our version of the model, we retain inertial terms, and we do not include any externally imposed randomness or spatial inhomogeneity. The system satisfies a nonlinear massive wave equation, given by

$$\frac{\partial^2 U}{\partial t^2} = \xi^2 \nabla^2 U - U - D(y)\phi \left[2\alpha \left[\frac{\partial U}{\partial t} + \nu \right] \right]. \quad (2)$$

The finite-difference approximation to (2) consists of a uniform lattice of blocks and springs (see Fig. 1), each displaced a dimensionless distance $U(x, y, t)$ from equilibrium with respect to the fixed upper surface, which represents the right side of a lateral fault. Here $U(x, y, t) \equiv U_{i,j}(t)$ is the displacement of the i, j th block on the lattice; the equilibrium block spacing is a , so that $x = ia$ (the horizontal axis for a lateral fault) and $y = ja$ (the depth) have the dimensions of length. Each block is attached to the upper surface with a harmonic pulling spring and to its nearest neighbors with harmonic coupling springs—the strength of the coupling springs relative to the pulling springs is $(\xi/a)^2$, where ξ is the stiffness length. The parameter ξ is also the sound speed

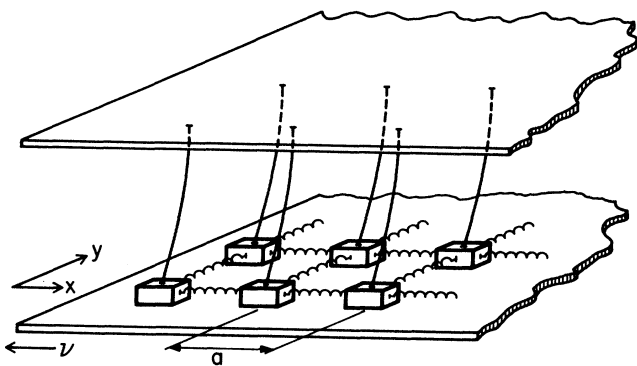


FIG. 1. Two-dimensional Burridge-Knopoff model consists of a lattice of blocks and springs in which displacements represent deformations of the fault surface. In the figure the x axis represents the horizontal axis of a lateral fault (the relative motion is parallel to the x axis) and the y axis represents the direction of increasing depth. The equilibrium block spacing is a in both directions. For our simulations we set $a=1$. N_x is the number of blocks in the x direction, and N_y is the number of blocks in the y direction. We use periodic boundary conditions in the x direction and free boundary conditions in the y direction. Our results are not sensitive to whether the boundary conditions are free or periodic, except for the depth-dependent models in the y direction, where periodic boundary conditions are unphysical.

since time is dimensionless. For numerical expedience we only allow lateral displacements; that is, blocks slip only in the x direction so that U is a scalar. We expect that this approximation to the actual elastic properties of the system will not greatly alter the statistical features that we study. Each block is in contact with a lower surface (corresponding to the left side of a lateral fault), which is moving slowly at a relative velocity of $-\nu$ with respect to the fixed surface. This loosely represents the effects of plate motion, which results in a slow shear deformation on opposite sides of the fault. The friction ϕ between the blocks and moving surface is a function only of the slip velocity and satisfies a velocity-weakening slip-stick friction law illustrated in Fig. 2. Each block remains stuck until its static friction exceeds the dimensionless threshold of unity, at which time the block becomes unstable and begins to slip with initial velocity proportional to σ . The rate of velocity weakening is given by α , so that larger values of α correspond to a steeper slope in the friction law and, hence, less dissipation. A straightforward linear stability analysis of spatially homogeneous solutions of Eq. (2) shows that small irregularities will be amplified exponentially at a rate proportional to α during slipping events [2].

In the depth-dependent model, we multiply the friction ϕ by a depth-dependent constant $D(y)$, which increases linearly with depth, corresponding the y axis in Fig. 1. Note that, because it multiplies the entire friction law,

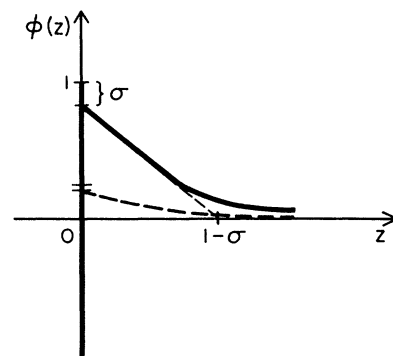


FIG. 2. Velocity-weakening slip-stick friction law $\phi(z)$ is represented by the solid line [the argument z can be obtained from Eq. (2)]. Sticking friction $\phi(0)$ satisfies $\phi(0) \leq 1$, while slipping friction decays monotonically to zero from the initial value $\phi(0^+) = 1 - \sigma$ with initial slope equal to -1 . The heavy dashed line represents the depth-dependent friction $D(y)\phi(z)$ at the top ($y=1$) of the depth-dependent model, while the solid line is the value of $D(y)\phi(z)$ at the bottom ($y=N_y$). For our simulations we take

$$\phi(z) = \begin{cases} (-\infty, 1], & z=0 \\ (1-\sigma)/\{1+[z/(1-\sigma)]\}, & z>0, \end{cases}$$

and $D(y) = 1/4[1 + 3(y-1)/(N_y-1)]$.

the factor $D(y)$ effectively alters the friction threshold, the initial impulse acting on slipping blocks, and the velocity-weakening parameter, which are now given by $D(y)$, $D(y)\sigma$, and $D(y)\alpha$, respectively. For our numerical simulations, we will take $D(y)$ to increase linearly from some minimum value at the top ($y=1$) of the model fault to some maximum value at the bottom ($y=N_y$); the extreme values are illustrated in Fig. 2. Here we account only for the increasing pressure as a function of depth, represented in the simplest possible way [10]. We ignore features such as pore pressure and temperature, which are also expected to vary with depth. We restrict our attention to the brittle zone, ignoring the brittle-to-ductile transition. We plan to incorporate these additional features in future versions of the model.

For our simulations we begin with some small spatial irregularities in the configuration and let the system evolve through several loading cycles (i.e., cycles of large events) until it reaches a statistically steady state. We study the limit of infinitesimally slow driving speeds ν in which slipping events occur one at a time. When the entire system is stuck, we determine which block is closest to threshold and then integrate (2) forward, updating the system so that this block comes to threshold in one step. At that point this least stable block begins to slip, with an initial impulse force of σ [or $D(y)\sigma$ in the depth-dependent friction model]. The event proceeds as we integrate Eq. (2) with $\nu=0$ until all blocks have come to rest. While the exact sequence of events will depend on the initial configuration, the statistical properties are in-

dependent of it.

The quantity used to gauge the size of each slipping event is called the moment and is given by the sum of the displacements of the blocks that move:

$$M = \int \Delta U(x,y) dx dy . \quad (3)$$

The magnitude μ is the natural logarithm of the moment: $\mu = \ln M$. In Fig. 3 we plot our numerical results for the rate of events $R(\mu)$ as a function of μ . Here $R(\mu)$ is the number of events per unit displacement per unit area (or length in one dimension) of the fault. Figures 3(a) illustrates our previous results for the one-dimensional model. Figure 3(b) illustrates our results for the homogeneous two-dimensional model. Figures 3(c) and 3(d) illustrate

our results for the two-dimensional model with depth-dependent friction—in Fig. 3(c) the fault is relatively deep, while in Fig. 3(d) the fault is relatively shallow. Most strikingly, for a wide range of parameters in all four cases, the scaling region, consisting of events of magnitude less than a crossover $\tilde{\mu}$, satisfies the Gutenberg-Richter law (1) with $b \approx 1$. In addition, in each case the large events with $\tilde{\mu} \leq \mu \leq \mu^*$ occur at a rate in excess of the extrapolated rate for small events. For all of our measurements, we find that the upper cutoff μ^* is quite sharp. In one dimension we found that for large enough systems μ^* is independent of system size; we expect this will also be the case in two dimensions (in our simulations even the largest events do not span the entire system), although the two-dimensional systems we study are not yet

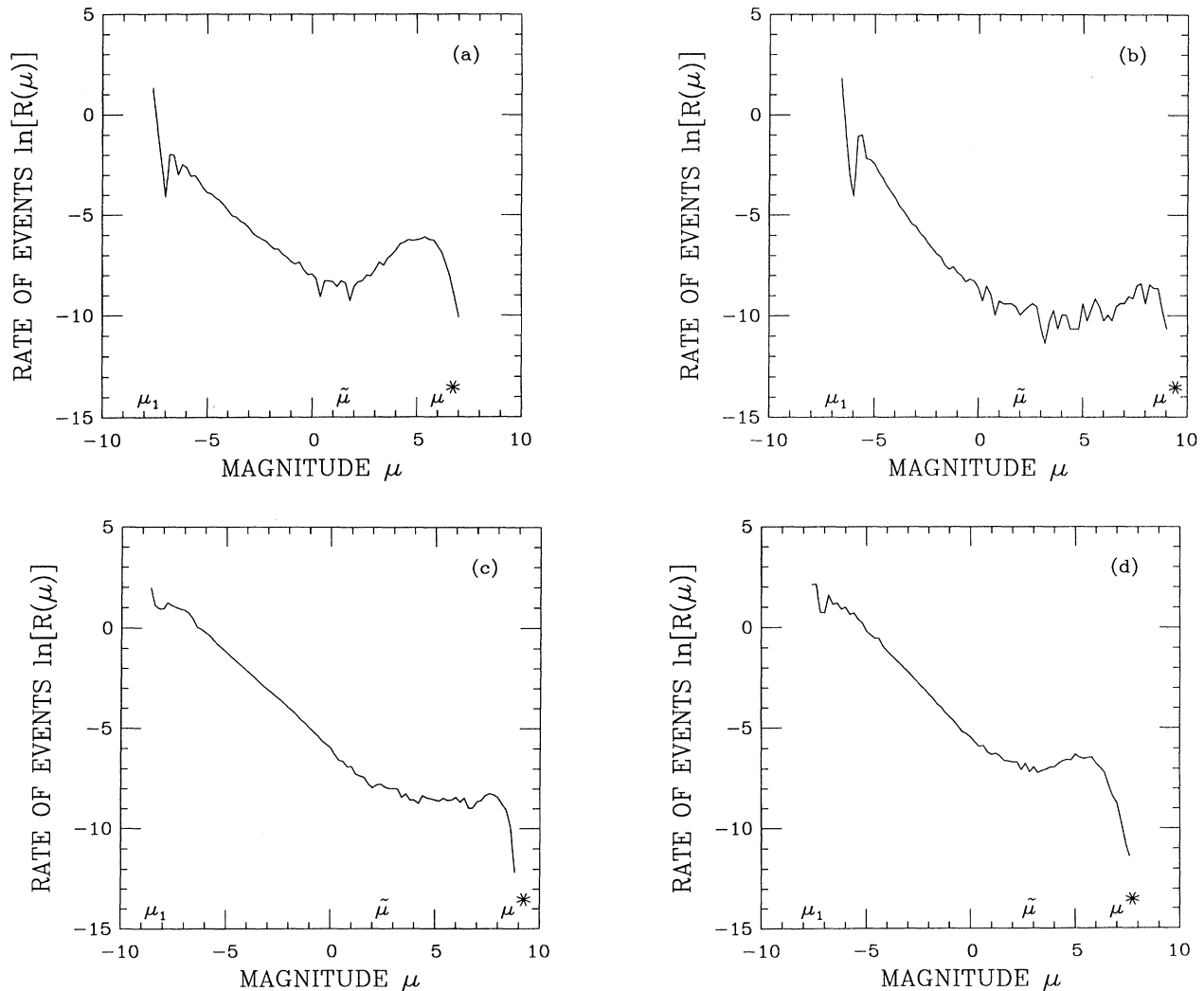


FIG. 3. Magnitude-vs-frequency distributions for (a) the one-dimensional model ($N=1500$, $\xi=6$, $\alpha=2.5$, and $\sigma=0.01$), (b) the spatially homogeneous two-dimensional model ($N_x=200$, $N_y=100$, $\xi=3$, $\alpha=2.5$, and $\sigma=0.01$), (c) the deep two-dimensional model with depth-dependent friction ($N_x=200$, $N_y=100$, $\xi=3$, $\alpha=2.5$, and $\sigma=0.01$), and (d) the shallow two-dimensional model with depth-dependent friction ($N_x=500$, $N_y=20$, $\xi=2$, $\alpha=2.5$, and $\sigma=0.01$). The smaller localized events range in magnitude from μ_1 (a one block event) to the crossover value $\tilde{\mu}$, and the delocalized events range in magnitude from $\tilde{\mu}$ to some upper cutoff μ^* . Most strikingly, in all four cases the distribution of localized events is characterized by a b value of unity.

large enough for us to systematically test this prediction.

The most pronounced differences between the statistical distributions presented in Fig. 3 are associated with the distributions of large events. In the one-dimensional model [Fig. 3(a)] and shallow fault [Fig. 3(d)], the distributions of large events are peaked near the upper cutoff μ^* , while for the homogeneous model [Fig. 3(b)] and deep fault [Fig. 3(c)], the distributions of large events are relatively flat. We expect that the peak seen in Fig. 3(d) reflects the fact that it is sufficiently shallow that it retains certain one-dimensional qualities.

Figure 4 (top) illustrates the slip distribution [13] in a typical delocalized large event for the shallow fault with depth-dependent friction. Note that the slipping region extends from the top to bottom, consistent with our interpretation of this case as quasi-one-dimensional. This event is triggered near the upper left corner, spreads from top to bottom of the fault, and then propagates unilaterally to the right, as shown in Fig. 4 (bottom), which illustrates the slipping blocks at equal intervals in time. Note that at any given time, only a small portion of the fault is slipping.

Similarly, for the deep fault, with and without depth-dependent friction, large events consist of narrow propagating front [6,7]. In these cases the fronts tend to propagate both horizontally and vertically; however, slipping zones are typically not at all spherically symmetric. Figure 5 illustrates a typical large event in the deep fault with depth-dependent friction. The event is triggered

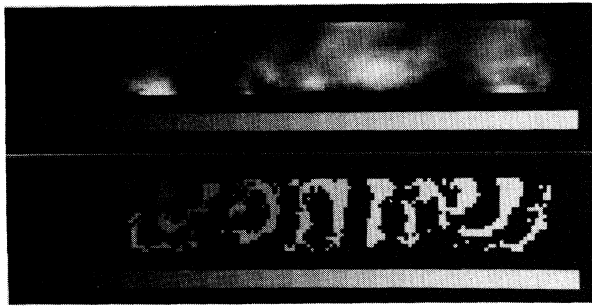


FIG. 4. Typical delocalized event in the shallow two-dimensional model with depth-dependent friction. The event has $\mu=6$, which is near the peak of the corresponding magnitude-vs-frequency distribution [the parameters are given in Fig. 3(d)]. In this event 2225 of the 10000 blocks are involved. The top figure illustrates the slip distribution in the event. Only the region near the slip is shown, corresponding to about 150 blocks along the x axis (the actual length of the fault is $N_x=500$). The shading illustrates the amount of slip during the event with black corresponding to no slip and the grey-to-white scale (shown under the figure) ranging linearly in displacement up to the maximum value of 0.6 during the event. The bottom figure illustrates the slipping blocks at equal intervals of time ($\Delta t=5$, in our dimensionless units, where the total duration is $t=75$), where grey corresponds to the earliest times, and white to the latest times during the event. Only a narrow band of blocks is slipping at any given time, and the event propagates primarily from left to right in the figure.

near the bottom of the fault, propagates initially upward and to the right, and then turns back down again toward the bottom.

In both Figs. 4 and 5 the events consist primarily of a single dominant front which propagates through the system. This is not always the case. Frequently, large events consist of two or more propagating fronts. Initially, events develop in a triggering zone in which a collection of blocks is near threshold. One or more large fronts emerge from this initial zone. For the shallow fault large events always consist of unilateral or bilateral propagating fronts. However, for the deep fault a front may encounter a firmly stuck region which is significantly smaller than the length of the front. This can lead to splitting of the front and, consequently, to more complex events.

Our measurements indicate that the value of the crossover moment \bar{M} in the magnitude-versus-frequency distribution is different in one and two dimensions. However, this is expected from dimensional analysis, which leads to an estimate of how \bar{M} scales with the parameter ξ . From Eq. (3) in one dimension (1D) the dimensions of

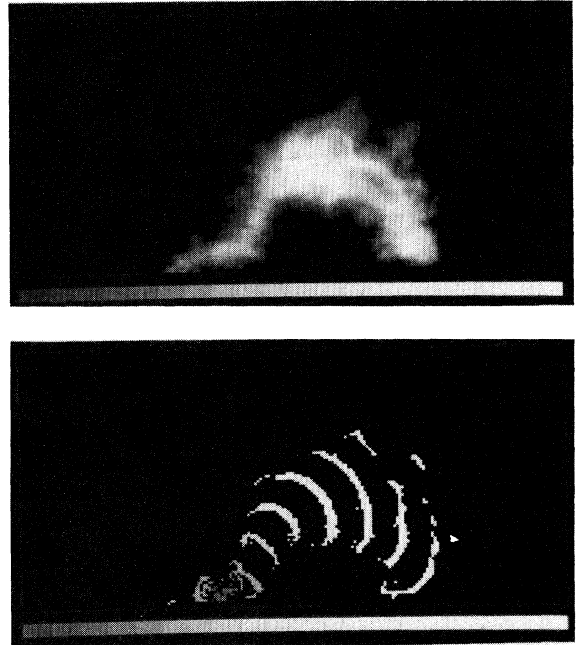


FIG. 5. Typical delocalized event in the deep depth-dependent model [parameter values as in Fig. 3(c)]. This event has $\mu=6$, which on the corresponding magnitude-vs-frequency distribution lies a little more than halfway between $\bar{\mu}$ and μ^* . In this event 3522 of the 20000 blocks are involved. The top figure illustrates the slip distribution during the event. The entire fault is shown. Black corresponds to no slip, while the grey-to-white scale ranges linearly up to the maximum displacement of 0.5 during the event. The bottom figure illustrates the slipping blocks at equal intervals of time ($\Delta t=5$, and the total duration is $t=44$), grey corresponding to early times and white corresponding to the latest times during the event.

moment are given by

$$[M_{1D}] = [\text{displacement}][\text{length}], \quad (4)$$

while in two dimensions,

$$\begin{aligned} [M_{2D}] &= [\text{displacement}][\text{area}] \\ &= [\text{displacement}][\text{length}]^2. \end{aligned} \quad (5)$$

In Eq. (2), U is the displacement, which is dimensionless, while ξ is the only parameter with the dimensions of length. Of course, the lattice spacing a and system length along the x or y axis, e.g., $L_x = N_x a$, where N_x is the number of blocks along the x axis, also have the dimensions of length; however, it seems reasonable to assume that the crossover \tilde{M} will not depend strongly on a or L for systems that are sufficiently large. Thus it follows that

$$\tilde{M}_{1D} \propto \xi, \quad \tilde{M}_{2D} \propto \xi^2, \quad (6)$$

with dimensionless corrections. For the one-dimensional model this scaling was verified in Ref. [5], and our two-dimensional simulations indicate that (6) gives a reasonably good fit to the data as ξ is varied [14].

Additional comparisons between the behavior of the two-dimensional depth-dependent model and seismicity patterns observed for real faults are obtained by examining the distribution of hypocenters and the magnitude-versus-frequency distribution as a function of depth. For a given earthquake the hypocenter is the position of the first motion detected by a seismograph (the epicenter refers to the position projected onto the Earth's surface). Study of the patterns of events may ultimately be useful for earthquake prediction. In the one-dimensional model we found that prior to a large event the maximum activity (largest rate of smaller events) was typically near the epicenter of the large event [4]. In the two-dimensional model our numerical simulations again show increased activity in the neighborhood of a coming large event. However, here we address the depth-dependent features of the hypocenter distribution to determine what types of potentially observable features might arise naturally as a consequence of increasing pressure as a function of depth.

In measurements of earthquake hypocenters and epicenters, there is an intrinsic uncertainty which arises from the fact that the threshold for detectable radiation from a given source depends somewhat on the distance of the measuring apparatus from the source. For that reason measurements are best obtained using near-field equipment, which is only available in certain locations [15]. The most reliable data on microearthquakes is obtained from near-field measurements. For large events one typically relies on far-field measurements, simply because few, if any, large events have occurred in locations where local seismographs are in place.

For the model we have calculated the magnitude-versus-frequency distribution as function of hypocenter depth, simulating near-field measurements by identifying the event hypocenter as the first block that moves and far-field measurements by identifying the hypocenter as the first block that moves faster than a specified threshold

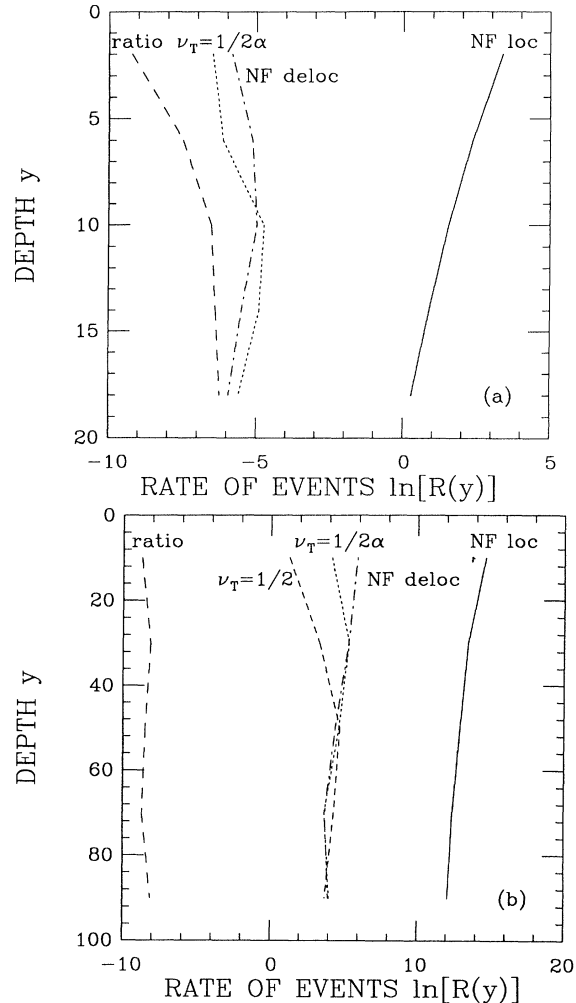


FIG. 6. Integrated magnitude-vs-frequency distributions as a function of depth for the depth-dependent models. In (a) we plot our results for the shallow fault [parameter values as in Fig. 3(d)], and in (b) we plot our results for the deep fault [parameter values as in Fig. 3(c)]. In each case the solid line represents near-field (NF) measurements of the localized events and corresponds to the total rate of events as a function of the depth of the first block that slips. The dot-dashed line represents the near-field measurements of the delocalized events. Here we only count events with magnitude greater than $\bar{\mu}$, as estimated from the corresponding magnitude-vs-frequency distribution (Fig. 3). In each case these measurements indicate that the localized events are increasingly suppressed with depth, while the rate of delocalized events is not very sensitive to depth. The ratio of near-field measurement of delocalized to localized events (long-dashed line) shows an enhanced relative rate of delocalized events with depth, especially in the case of the shallow fault. The dotted line represents the far-field measurements of delocalized events, which is the rate of delocalized events as a function of the depth at which the velocity first exceeds $\nu_T = 1/(2\alpha)$. The shallow fault [(a)] shows an enhanced rate of delocalized events using this far-field measurement, while on such enhancement is seen for the deep fault [(b)]. In order to obtain a similar enhancement for the deep fault, a much larger velocity threshold must be used. The medium-length dashed line in (b) shows the result of far-field measurements for delocalized events in which the velocity threshold is taken to be $\nu_T = \frac{1}{2}$.

velocity, taken here to be $1/(2\alpha)$. The near-field measurements thus correspond to a much smaller detection threshold. We expect that measurements based on an acceleration threshold would give qualitatively similar results.

The results of our simulations are illustrated in Fig. 6, where we plot integrated magnitude-versus-frequency distributions as a function of depth for several different cases. Our “near-field” measurements for the total rate of events (including events of all sizes) indicate that for both the deep and shallow faults, overall, more events are triggered near the surface, as should be expected since the friction threshold is least at the top. Because the smaller localized events dominate the overall number of events, this measurement indicates an enhanced rate of smaller events near the surface. In contrast, a separate near-field plot which includes only the delocalized events ($\mu \geq \bar{\mu}$) indicates that the hypocenters of delocalized events occur at a more nearly uniform, depth-independent rate, with a small enhancement near the surface. For comparison, the ratio of the near-field rate of delocalized to localized events is also plotted. The ratio shows a strong enhancement with depth in the case of the shallow fault, indicating that, relative to the rate of smaller events, the large events are much more likely to be triggered at depth. For the deep fault the relative rate still appears to be rather uniform with depth.

In contrast, even before any ratios are taken, under certain circumstances the “far-field” measurements show an enhanced rate of hypocenters of large events with increasing depth. For the shallow fault the enhancement is seen when the threshold velocity is taken to be $v_T = 1/(2\alpha)$. For the deep fault the threshold $v_T = 1/(2\alpha)$ does not lead to an enhanced rate of large events with increasing depth. Instead, a much larger threshold (which is probably unphysically large as a detection threshold) must be specified in order for the enhancement to be observed. This is due to at least in part to the fact that, for the deep fault, even a large event ($\mu > \bar{\mu}$) need not contact the bottom at all. See Fig. 7 for an example of this behavior. Generally, our results indicate that while the actual first motions are equally likely at any depth, the first fastest slipping speeds are somewhat more likely to be obtained at depth in the model.

These results can be compared with the data of Sibson [11] for the hypocenter distributions of microearthquakes and focal depths of large earthquakes in various different regions of California. Sibson’s main conclusion is that the rate of microearthquakes begins to decrease below a certain depth in the crust and that large events tend to be triggered at depths where the rate of microearthquakes has decreased substantially. In general, the observed behavior and relevant depths vary regionally, as does the focal depth of the large earthquake relative to the tail of the distribution of smaller events. Here we will comment on only the most general patterns. Our near-field measurements of localized events in the model, in which we saw a decreasing rate of these events as a function of depth, are qualitatively consistent with Sibson’s measurements of the decreasing rate of microearthquakes with depth. Sibson’s data also show that typically there is rel-

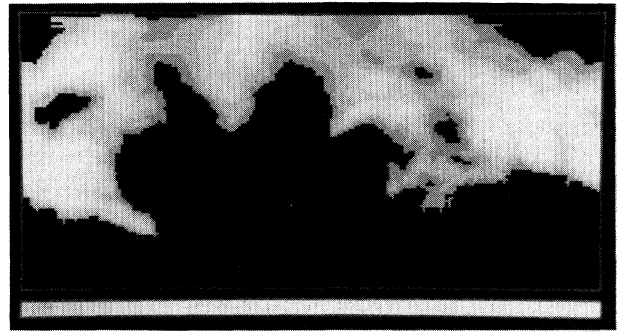


FIG. 7. Slip distribution in a delocalized event in the deep depth-dependent model [parameters as in Fig. 3(c)]. Shading from grey to white indicates increased displacement, while black regions did not slip at all. This event has $\mu = 7$ and spans the system from left to right, but not from top to bottom. In fact, in this event the bottom of the fault does not slip at all.

atively little seismic activity at very shallow depths (up to 5 or so kilometers), a behavior that is absent in the model. We expect that this discrepancy arises from material properties near the surface of the crust which have been left out of the model and associate the “top” of our model fault with the depth at which seismic activity peaks. The relationship between the data and our results for the model is less clear in the case of large events. Our results compare most favorably in the case of the shallow fault, where the far-field measurements showed that large events tend to be triggered at depth. It is difficult at this point to tell whether the discrepancies between the data and our results for the deep fault arise because the crust depth in California is more comparable to the dimensions of the shallow fault or whether the discrepancy is due to features such as the brittle-to-ductile transition in the crust, which have been left out of the model.

In summary, we have shown that the two-dimensional version of a Burridge-Knopoff model gives rise to a magnitude-versus-frequency distribution which is characterized by a b value of unity describing the smaller localized events and an excess of large events, consistent with results obtained for real faults [16,17]. We have also made some preliminary studies of a generalization of the original spatially homogeneous model to one in which the friction depends on depth. Comparisons can be made between our displacement patterns and Archuleta’s kinematic reconstructions of real events [13] and our results for the hypocenter distribution and Sibson’s data for hypocenter distributions on real faults [11].

In the one-dimensional version of the model, we observed [2] a crossover in the magnitude-versus-frequency distribution corresponding to the transition between localized and delocalized events. In the Earth this crossover is associated with the depth of the crust and a crossover which occurs when an event just breaks the current from top to bottom [10]. Based on estimates of the parameters in the model [5] (obtained from data for microearthquakes [15] and typical sound speeds and slip

times in the crust), we obtained an estimate of the crossover magnitude predicted by the model which is consistent with the corresponding estimate based on crust depth. It is not at all clear why such different mechanisms lead to such similar predictions. Interestingly, comparisons between the numbers used in these estimates indicate that the depth of faults in California (approximately 15 km) and the length scale in the model, $\tilde{\xi} = 2\xi/\alpha \ln(4\xi^2/\sigma a)$, at which the crossover between localized and delocalized events takes place, are roughly equal.

Our two-dimensional simulations again showed a crossover in the magnitude-versus-frequency distribution which distinguished between localized and delocalized events. Our results for the deep fault, in which most of the large events did not span the fault from top to bottom, indicate that in the model this crossover is not depth dependent. Interestingly, however, in our simulations of the shallow fault, the depth ($N_y = 20$) is roughly equal to the crossover length [18] ($\tilde{\xi} = 15$), and it was this case that had the best agreement with the California hypocenter distribution data. In contrast, for the deep fault the depth ($N_y = 100$) was substantially greater than the crossover length ($\tilde{\xi} = 20$). The correspondence between the observed depth-dependent crossover in the Earth and the transition in the model remains an interesting and important question.

Of course, the sense in which our results agree with data at this point is purely qualitative. For example, for a more quantitative comparison of the hypocenter distributions, it would be necessary to carefully choose the dimensions of the model system, the depth dependence of the friction law, and other model parameters to corre-

spond to realistic values. However, so many potentially important features have been left out of the model that such a detailed investigation would at this point be premature. First, we plan to determine the qualitative changes in behavior which occur when various different realistic features are added to the model. Another important feature that may enhance the depth-dependent patterns is the variation of temperature with depth, which results in the brittle-to-ductile transition in the crust. This transition, which marks the interface between the mantle and crust, might be incorporated in the model by adding a viscous region, corresponding to a velocity-strengthening friction law, below a certain depth [10,19]. It is conceivable that this feature may also lead to an enhanced rate to large events at depth. Ultimately, the most useful models may be based on insights gained by contrasting the changes in behavior produced by adding different complexities both individually and collectively. This work represents the first step in a program aimed at constructing more realistic models.

The fact that in all of the generalizations of the model that we have considered so far the b value of unity first seen in one-dimension persists of two-dimensions is a very promising feature of this model, because it is consistent with available data. The robustness of this result suggests that it should follow from rather general considerations and remains an outstanding and provocative question for the model.

In the course of this work I have benefited from many useful discussions with James Langer, Chris Myers, Craig Nicholson, Bruce Shaw, and Chao Tang.

-
- [1] J. M. Carlson and J. S. Langer, *Phys. Rev. Lett.* **62**, 2632 (1989).
- [2] J. M. Carlson and J. S. Langer, *Phys. Rev. A* **40**, 6470 (1989).
- [3] J. M. Carlson, *J. Geophys. Res.* **96**, 4255 (1991).
- [4] B. Shaw, J. M. Carlson, and J. S. Langer (unpublished).
- [5] J. M. Carlson, J. S. Langer, B. Shaw, and C. Tang, *Phys. Rev. A* **44**, 884 (1991).
- [6] B. Shaw (unpublished).
- [7] J. S. Langer and C. Tang, *Phys. Rev. Lett.* **67**, 1043 (1991).
- [8] See, for example, B. Gutenberg and C. F. Richter, *Seismicity of the Earth and Related Phenomena* (Princeton University Press, Princeton, 1954).
- [9] See, for example, S. G. Wesnousky, C. H. Scholz, K. Shimazaki, and T. Matsuda, *J. Geophys. Res.* **88**, 9331 (1983); S. Singh, M. Rodriguez, and L. Esteva, *Bull. Seismol. Soc. Am.* **73**, 1779 (1983); D. P. Schwartz and K. J. Coppersmith, *J. Geophys. Res.* **89**, 5681 (1984); F. C. Davison and C. H. Scholz, *Bull. Seismol. Soc. Am.* **75**, 1349 (1985).
- [10] See, for example, C. H. Scholz, *The Mechanics of Earthquakes and Faulting* (Cambridge University Press, New York, 1990).
- [11] R. H. Sibson, *Bull. Seismol. Soc. Am.* **72**, 151 (1982).
- [12] R. Burridge and L. Knopoff, *Bull. Seismol. Soc. Am.* **57**, 341 (1967).
- [13] To compare these results with reconstructions of displacement and propagation patterns of real earthquakes, see R. Archuleta, *J. Geophys. Res.* **89**, 4559 (1984).
- [14] A better estimate of the crossover moment in one dimension was obtained in Ref. [2] and is given by $\tilde{M}_{1D} = 2\xi/\alpha$. This agrees with (6), but includes a dimensionless coefficient. The corresponding calculation can easily be repeated for the two-dimensional model (without depth-dependent friction); however, the results depend on assumptions made about the shape of the initial triggering zone. Assuming radial symmetry, we obtain $\tilde{M}_{2D} = 2\xi\tilde{\xi}/\alpha$, where $\tilde{\xi} = (2\xi/\alpha)\ln(4\xi^2/\sigma a^2)$, which differs from (6) by a logarithmic correction.
- [15] P. E. Malin, S. N. Blakeslee, M. G. Alvarez, and A. J. Martin, *Science* **244**, 557 (1989).
- [16] H. Kanamori and D. L. Anderson, *Bull. Seismol. Soc. Am.* **65**, 1073 (1975).
- [17] G. Ekstrom and A. M. Dziewonski, *Nature* **332**, 319 (1988).
- [18] Our calculation of $\tilde{\xi}$, and consequently this estimate, ignores depth dependence.
- [19] S. T. Tse and J. R. Rice, *J. Geophys. Res.* **91**, 9452 (1986).



FIG. 4. Typical delocalized event in the shallow two-dimensional model with depth-dependent friction. The event has $\mu=6$, which is near the peak of the corresponding magnitude-vs-frequency distribution [the parameters are given in Fig. 3(d)]. In this event 2225 of the 10 000 blocks are involved. The top figure illustrates the slip distribution in the event. Only the region near the slip is shown, corresponding to about 150 blocks along the x axis (the actual length of the fault is $N_x=500$). The shading illustrates the amount of slip during the event with black corresponding to no slip and the grey-to-white scale (shown under the figure) ranging linearly in displacement up to the maximum value of 0.6 during the event. The bottom figure illustrates the slipping blocks at equal intervals of time ($\Delta t=5$, in our dimensionless units, where the total duration is $t=75$), where grey corresponds to the earliest times, and white to the latest times during the event. Only a narrow band of blocks is slipping at any given time, and the event propagates primarily from left to right in the figure.

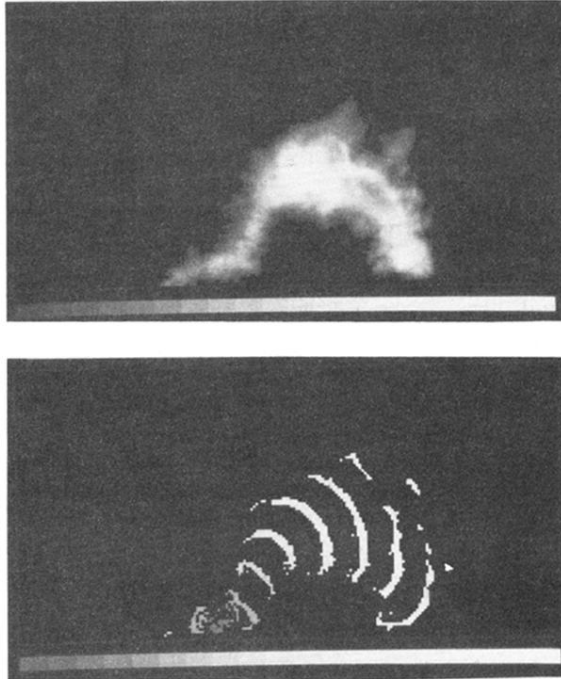


FIG. 5. Typical delocalized event in the deep depth-dependent model [parameter values as in Fig. 3(c)]. This event has $\mu=6$, which on the corresponding magnitude-vs-frequency distribution lies a little more than halfway between $\bar{\mu}$ and μ^* . In this event 3522 of the 20 000 blocks are involved. The top figure illustrates the slip distribution during the event. The entire fault is shown. Black corresponds to no slip, while the grey-to-white scale ranges linearly up to the maximum displacement of 0.5 during the event. The bottom figure illustrates the slipping blocks at equal intervals of time ($\Delta t=5$, and the total duration is $t=44$), grey corresponding to early times and white corresponding to the latest times during the event.

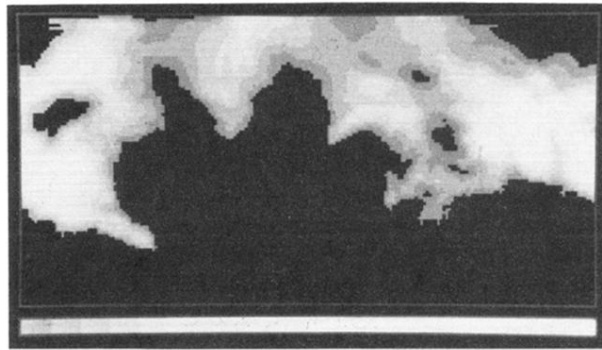


FIG. 7. Slip distribution in a delocalized event in the deep depth-dependent model [parameters as in Fig. 3(c)]. Shading from grey to white indicates increased displacement, while black regions did not slip at all. This event has $\mu=7$ and spans the system from left to right, but not from top to bottom. In fact, in this event the bottom of the fault does not slip at all.